# Fast and slow microphysics regimes in a minimalist model of cloudy Rayleigh-Bénard convection

Raymond A. Shaw [1,*] Subin Thomas [1] Prasanth Prabhakaran [1,†] Will Cantrell [1]
Mikhail Ovchinnikov [2] and Fan Yang [3]
[1]*Department of Physics, Michigan Technological University, Houghton, Michigan 49931, USA*
[2]*Pacific Northwest National Laboratory, Richland, Washington 99352, USA*
[3]*Brookhaven National Laboratory, Upton, New York 11973, USA*

(Received 6 May 2023; accepted 5 September 2023; published 6 October 2023)

A minimalist model of microphysical properties in cloudy Rayleigh-Bénard convection is developed based on mass and number balances for cloud droplets growing by vapor condensation. The model is relevant to a turbulent mixed-layer in which a steady forcing of supersaturation can be defined, e.g., a model of the cloudy boundary layer or a convection-cloud chamber. The model assumes steady injection of aerosol particles that are activated to form cloud droplets, and the removal of cloud droplets through sedimentation. Simplifying assumptions include the consideration of mean properties in steady state, neglect of coalescence growth, and no detailed representation of the droplet size distribution. Closed-form expressions for cloud droplet radius, number concentration, and liquid water content are derived. Limits of fast and slow microphysics, compared to the turbulent mixing time scale, are explored, and resulting expressions for the scaling of microphysical properties in fast and slow regimes are obtained. Scaling of microphysics with layer thickness is also explored, suggesting that liquid water content and cloud droplet number concentration increase, and mean droplet radius decreases with increasing layer thickness. Finally, the analytical model is shown to compare favorably to solutions of the fully-coupled set of governing ordinary differential equations that describe the system, and the predicted power law for liquid water mixing ratio versus droplet activation rate is observed to be consistent with measurements from the Pi convection-cloud chamber.

DOI: 10.1103/PhysRevResearch.5.043018

## I. INTRODUCTION

For over 50 years the turbulent mixed layer has been the predominant paradigm for our understanding of stratocumulus clouds [1–10]. The microphysical properties of these extensive decks of low clouds are crucial to our understanding of climate [11]. Furthermore, microphysical processes influence the optical properties and persistence of stratocumulus clouds [12–14], as well as other related systems like mixed-phase layer clouds [15] and fog [16].

Distilled to its essence, the physics of a shallow layer cloud in steady state includes (1) a constant driving force for water supersaturation, for example, resulting from the updrafts of the turbulent circulation within the boundary layer; (2) a steady source of aerosol particles that can act as cloud condensation nuclei (CCN); (3) cloud microphysical processes, including activation to form cloud droplets, and growth of cloud droplets by condensation and possibly by collision and coalescence; (4) a steady loss of particles, for example through sedimentation [14]. The purpose of this paper is to develop a minimalist, mean-field (zero-dimensional) model that will allow us to demonstrate the existence of and explore the properties of fast and slow microphysical regimes that result from these essential elements. We take moist Rayleigh-Bénard convection with a fixed temperature gradient as an idealized framework, thereby not allowing the microphysics to feed back to the dynamics. The work will be framed in the context of turbulent clouds formed in a laboratory convection-cloud chamber, which can be related to atmospheric systems by using dimensionless variables for the microphysics [17]. Indeed, the Damkoehler number emerges from the analysis as the central dimensionless quantity governing the boundary between fast and slow microphysical regimes. The exact details of the forcing and the particle-loss terms may be different for a particular cloud system, but fast and slow regimes with corresponding scaling laws for microphysical properties will still exist.

A convection-cloud chamber allows for the formation of a steady-state cloud, with a balance between aerosol injection, their activation as cloud droplets, growth by condensation, and eventually their loss by sedimentation [18]. The microphysical properties of the cloud within the chamber, including even "bulk" quantities like liquid water content, depend on the properties of the injected aerosols [19]. We develop a simple model to calculate the liquid water content and other microphysical properties (e.g., cloud droplet concentration and mean radius, and water vapor supersaturation) corresponding to a given aerosol injection rate and imposed supersaturation forcing. The number-mass approach is inspired by that of Krueger [20], and the mean-field approach has been shown

*rashaw@mtu.edu
†CIRES, University of Colorado and NOAA/Chemical Sciences Laboratory, Boulder, Colorado, USA.

to compare favorably with more complex, three-dimensional models [21,22]. The paper proceeds as follows. First, an analytical model is developed for the steady-state properties, and it is interpreted in the limits of fast and slow cloud microphysics relative to the turbulent mixing in the mixed layer. Analytical scaling relationships between microphysical variables are obtained, and in particular we investigate dependence on the depth of the mixed layer. Second, the analytical results are shown to match results from a time-dependent model based on a coupled set of ordinary differential equations. Third, we compare the predicted scaling of liquid water content to measurements in the Pi convection-cloud chamber [23]. Finally, we conclude with a discussion of the relevant dimensionless variables, the connection to bulk microphysics with saturation adjustment, and aspects for future work.

## II. THERMODYNAMIC MODEL FOR MOIST RAYLEIGH-BÉNARD CONVECTION

The thermodynamics state within a turbulent convective layer, such as that occurs in a convection chamber, is obtained using the mean-field approach described by Thomas *et al.* [21]. It is assumed that the fluid in the turbulent convection layer is well mixed at temperature $T$. With no condensation, the time rate of change of the temperature of the well-mixed air can simplify to

$$\frac{dT}{dt} = \frac{1}{\tau_t}(T_0 - T) \tag{1}$$

where $T_0$ is the steady-state temperature that the fluid attempts to reach and $\tau_t$ is the characteristic time. For example, if we consider Rayleigh-Bénard convection with a bottom temperature of $T_b$ and a top temperature of $T_t$, $T_0 = (T_b + T_t)/2$ and $\tau_t = H\lambda/2\alpha$, where $H$ is the height of the layer, $\lambda$ is the thickness of the viscous boundary layer, and $\alpha$ is the thermal diffusivity of air (see Appendix A for a more detailed development). The solution to Eq. (1) is

$$T = T_i e^{-t/\tau_t} + T_0(1 - e^{-t/\tau_t}). \tag{2}$$

Thus, the temperature evolves from the initial value $T_i$ to the steady-state value $T_0$ at a characteristic time $\tau_t$. We can interpret $\tau_t$ as the turbulent-flux replenishment time of the system.

A similar equation can be written for the water vapor mixing ratio $q_v$ in well-mixed air. The evolution equation for water vapor mixing ratio is

$$\frac{dq_v}{dt} = \frac{1}{\tau_t}(q_{v0} - q_v), \tag{3}$$

where $q_{v0}$ is the steady-sate water vapor mixing ratio with no condensation. Similarly, in moist Rayleigh-Bénard convection, $q_{v0} = (q_{s,b} + q_{s,t})/2$, where $q_{s,b}$ and $q_{s,t}$ represent saturated water vapor pressure at bottom and top surfaces, respectively. Strictly speaking, the time scale in this case is equal to $2D/H\lambda$, where $D$ is the diffusion coefficient of water vapor in air, but practically speaking this can be taken as equal to $\tau_t$ because $D \approx \alpha$.

By analogy, a water vapor supersaturation equation, with no condensation, can be written as

$$\frac{ds}{dt} = \frac{1}{\tau_t}(s_0 - s), \tag{4}$$

where $s_0$ is the cloud-free value of the supersaturation corresponding to $q_{v0}$ and $T_0$. A justification of Eq. (4) is given in Appendix B; and the adequacy of Eq. (4) will be checked later both computationally and experimentally (see Sec. V). In moist Rayleigh-Bénard convection, an approximation of $s_0$, as detailed in Appendix A, is given by

$$s_0 = \frac{1}{2}\left(\frac{L\Delta T}{2R_v T_0^2}\right)^2, \tag{5}$$

where $\Delta T = T_b - T_t$, $L$ is the latent heat of vaporization, and $R_v$ is the gas constant for water vapor.

Equation (4) is fundamental to the microphysics within the turbulent layer, so it is worth noting several points now. First, when a cloud is present, such that $s$ is small, the right-hand side of Eq. (4) can be considered as a forcing term, equivalent to an updraft strength or radiative cooling, namely, the term that forces the development of supersaturation and the formation of a cloud. Second, when condensation occurs in the chamber the steady-state water vapor mixing field will be slightly depleted and the mean temperature will be slightly increased due to release of latent heat of vaporization. Those shifts are $\delta q_v = q_v - q_{v0}$ and $\delta T = T - T_0$, and expressions for these differences are given later. This can be included in Eq. (4) as a loss term due to cloud droplet growth. The full system is developed in Sec. III.

## III. MEAN-FIELD MODEL OF CLOUD MICROPHYSICAL PROPERTIES

We now consider cloud formation in the convective layer. The well-mixed, bulk fluid contains a cloud of droplets with radius $r$ and number density $n$. The cloud is maintained in steady state by injecting a constant flow of cloud condensation nuclei (CCN), such that the cloud droplet activation rate is equal to the rate at which droplets are removed by sedimentation. In the following subsections we consider a liquid-water mass budget and a cloud droplet number budget. The resulting equations are then combined to solve for $r$, $n$, and the liquid water content $m$.

### A. Liquid water mass budget

In steady state the rate of condensation is balanced by the rate of loss of mass due to sedimentation, $\dot{m}_{\rm cond} = \dot{m}_{\rm sed}$. The rate of change of liquid water mass per unit volume due to condensation, assuming fixed $n$, is given by

$$\dot{m}_{\rm cond} = n\rho_l 4\pi r\xi s. \tag{6}$$

The parameter $\xi$ is a weak function of temperature [24]. The rate of change of liquid water mass per unit volume due to the precipitation flux is

$$\dot{m}_{\rm sed} = m/\tau_{\rm res} = n\rho_l \frac{4}{3}\pi r^3 \frac{v_T}{H}, \tag{7}$$

where $v_T$ is the terminal speed of cloud droplets. Here we have assumed that the residence time of a cloud droplet is

$\tau_{\rm res} = H/v_T$. The terminal speed is assumed to follow Stokes drag law, such that $v_T = 2\rho_l g r^2/(9\mu)$, where $\mu$ is the dynamic viscosity of air and $g$ is the gravitational acceleration. This simple assumption for the removal time scale $\tau_{\rm res}$ is valid in the "stirred-settling" limit, and may need to be revised for drops with large inertia, etc. [25].

We observe that $\dot{m}_{\rm cond} = c_{\rm cond} nrs$ and $\dot{m}_{\rm sed} = c_{\rm sed} nr^5$, so we expect it should be possible to obtain an expression for $n$ as a function of $r$. As anticipated in the previous section, however, supersaturation depends on the condensation rate and therefore is also a function of $n$ and $r$. The supersaturation must be obtained by Eq. (4), but including a term accounting for depletion due to droplet growth [26]

$$\frac{ds}{dt} = \frac{1}{\tau_t}(s_0 - s) - \frac{s}{\tau_c}, \tag{8}$$

where $\tau_c$ is the phase relaxation time. It is given by

$$\tau_c = (4\pi D' nr)^{-1}, \tag{9}$$

where $D' = \rho_l \xi Q_2/\rho_{v,s}$. Here, $Q_2$ accounts for the decrease in supersaturation due to depletion of the water vapor mixing ratio due to droplet growth [26]. It follows then, that in steady state the supersaturation can be written as

$$s = s_0\left(1 + \frac{\tau_t}{\tau_c}\right)^{-1}. \tag{10}$$

By equating Eqs. (6) and (7) the expression for cloud droplet number density then becomes

$$n = \left(\frac{c_{\rm cond}}{c_{\rm sed}}\frac{s_0}{r^4} - 1\right)\frac{1}{\tau_t 4\pi D' r}. \tag{11}$$

Alternately, this can be expressed as

$$n = \left(\frac{\dot{m}_{\rm cond,0}}{\dot{m}_{\rm sed}} - 1\right)\frac{1}{\tau_t 4\pi D' r}, \tag{12}$$

where $\dot{m}_{\rm cond,0}$ is the condensation rate that would exist at the cloud-free supersaturation of $s_0$.

### B. Cloud droplet number budget

Again, steady state is assumed, such that the rate of CCN injection and activation is balanced by the rate of loss by sedimentation, $\dot{n}_{\rm in} = \dot{n}_{\rm sed}$. The rate of injection per unit volume $\dot{n}_{\rm in}$ is a constant that is externally controlled. The rate of loss through sedimentation is assumed to be proportional to $n/\tau_{\rm res}$, with the residence time defined in the previous section, such that

$$\dot{n}_{\rm sed} = n\frac{v_T}{H} = n\frac{2\rho_l g r^2}{9\mu H}. \tag{13}$$

Equating these rates and solving for $n$ results in

$$n = \dot{n}_{\rm in}\frac{9\mu H}{2\rho_l g}\frac{1}{r^2}. \tag{14}$$

### C. Solutions for microphysical properties

Equations (11) and (14) allow us to obtain a quartic equation for radius,

$$r^4 + \left(\frac{18\pi\mu H D' \tau_t \dot{n}_{\rm in}}{\rho_l g}\right)r^3 - \frac{27\xi\mu H s_0}{2\rho_l g} = 0. \tag{15}$$

For a quartic of the form $x^4 + a_3x^3 + a_0 = 0$ the discriminant is $\Delta = 256a_0^3 - 27a_3^4a_0^2$. Realistic values of the coefficients lead to $\Delta < 0$, ensuring that there are two distinct, real roots. In our case only one is positive, and therefore is the allowable solution.

Once a value for $r$ is obtained, it can be substituted into Eq. (14) or (11) to obtain the corresponding $n$. Then other microphysical properties can be calculated, such as supersaturation via Eqs. (9) and (10), and liquid water content $m = n\rho_l 4\pi r^3/3$.

Figure 1 shows the microphysical state of the system as a function of $\dot{n}_{\rm in}$, as obtained from the expressions derived in this section. The results correspond to $T_0 = 284.16$ K, $\Delta T = 20$ K, and $H = 1$ m. The supersaturation decreases with increasing $\dot{n}_{\rm in}$, approaching zero at high injection rate. The droplet number concentration increases and the droplet radius decreases with $\dot{n}_{\rm in}$ in such a way that the liquid water content increases monotonically. A distinct shift in the behavior of the system is observed between $\log \dot{n}_{\rm in}$ of $-2$ and $-1$, and these two microphysical regimes will be explored in Sec. IV.

### D. Maximum achievable $n$ and $m$: Threshold values for critical supersaturation

In practice there is a limit to the number concentration of cloud droplets that can be activated for a given set of parameters $\Delta T$ and $H$. This can be understood by assuming all injected CCN are identical and have a critical supersaturation of $s_c$. Then the injection rate will have a peak value at which the ambient supersaturation in the chamber is equal to $s_c$, and $r$, $n$ and $m$ reach maximum values. In that case we can write the mass condensation rate from Eq. (6) as

$$\dot{m}_{\rm cond} = n\rho_l 4\pi r\xi s_c. \tag{16}$$

Setting that equal to the sedimentation rate in Eq. (7) results in

$$n\rho_l 4\pi r\xi s_c = n\rho_l \frac{4}{3}\pi r^3 \frac{v_T}{H}, \tag{17}$$

and we see that $n$ cancels and we can solve for the radius corresponding to the critical supersaturation,

$$r_c = \left(\frac{27\xi\mu H s_c}{2\rho_l g}\right)^{1/4}. \tag{18}$$

This radius is the minimum value of cloud droplet radius that can be achieved in the chamber, when fluctuations in supersaturation are neglected. (When fluctuations exist, it is possible for CCN to be activated even when the mean supersaturation is below the critical value [19], but that case is not considered here.) The minimum radius, in turn, allows for maximum values of $n$ and $m$ to be obtained,

$$n_c = \frac{1}{4\pi D' \tau_t r_c}\left(\frac{s_0}{s_c} - 1\right) \tag{19}$$

and

$$m_c = \frac{\rho_l}{3D'\tau_t}\left(\frac{s_0}{s_c} - 1\right)r_c^2. \tag{20}$$

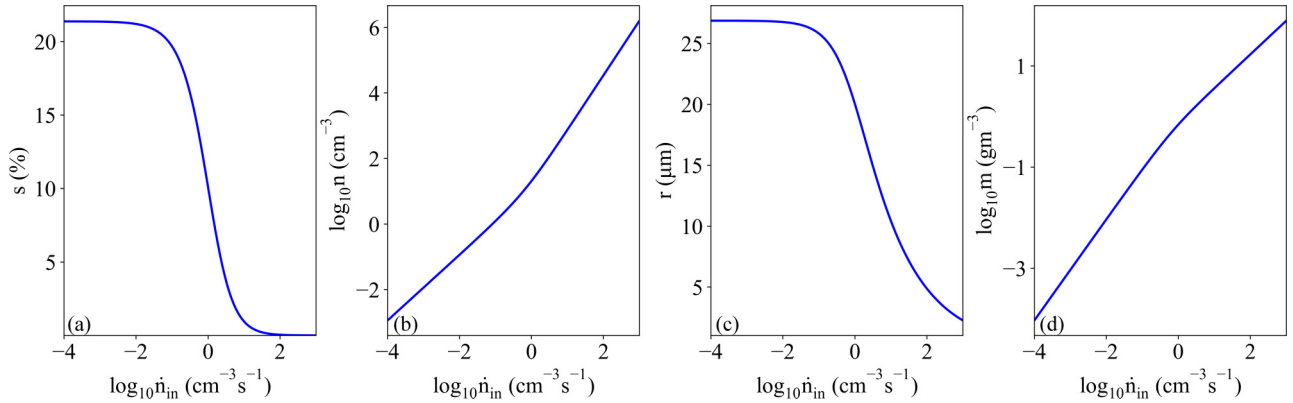


FIG. 1. The steady-state supersaturation, cloud droplet number concentration, mean droplet radius, and liquid water content are plotted against aerosol injection rate $\dot{n}_{\rm in}$. The parameters $\tau_t = 10$ s and $s_0 = 21.32\%$ are held constant. As the injection rate is increased the cloud droplet number concentration increases, consequently, mean supersaturation and mean radius of cloud droplets decrease.

These are the upper bounds on droplet number concentration and liquid water content in a turbulent convective layer, again neglecting fluctuations. Considering Fig. 1 for illustration, the first panel shows that $s$ approaches zero monotonically with increasing $\dot{n}_{\rm in}$. The second and fourth panels show the increasing $n$ and $m$, and the third panel shows the steadily decreasing $r$. In practice, the curves should end at the $\dot{n}_{\rm in}$ at which $s_c$ is reached.

## IV. FAST AND SLOW MICROPHYSICS REGIMES

### A. Fast-microphysics limit

Limiting microphysical scaling regimes are achieved for high and low CCN injection rates. We first consider the limit of fast microphysics (i.e., high CCN injection rate) compared to turbulent mixing, i.e., $\tau_t \gg \tau_c$. In that regime Eq. (10) becomes $s \approx s_0 \tau_c/\tau_t$. Then the mass condensation rate simplifies to

$$\dot{m}_{\rm cond} = n\rho_l 4\pi r \xi \frac{\tau_c}{\tau_t} s_0 = \frac{\rho_l \xi s_0}{D'\tau_t}, \tag{21}$$

where Eq. (9) was used to obtain the last equality. This result is striking because it is independent of microphysical properties, in other words, it contains no dependence on $n$ or $r$. In the fast-microphysics limit, therefore, the mass condensation rate is a constant that depends only on the maximum possible supersaturation $s_0$ and the turbulence intensity through $\tau_t$. The quantity $s_0/\tau_t$ can be considered the rate of replenishment of supersaturation in the chamber, which is the limit on condensation growth in this regime.

Equating $\dot{m}_{\rm cond} = \dot{m}_{\rm sed}$ using Eq. (7), we can obtain an expression for the cloud droplet number concentration,

$$n = \frac{27\xi s_0 \mu H}{8\pi D'\tau_t \rho_l g r^5}. \tag{22}$$

The $n \propto r^{-5}$ scaling can be observed in Fig. 2(a), where the plateau at large $\dot{n}_{\rm in}$ indicates the range over which the scaling holds (due to the compensated $y$ axis). Alternately, we can solve for cloud liquid water content,

$$m = \frac{9\mu\xi s_0 H}{2gD'\tau_t} r^{-2}, \tag{23}$$

which confirms that $m$ increases with decreasing $r$ and therefore with increasing CCN injection rate. Note that these expressions combine to give $m \propto n^{2/5}$. That scaling is observed in Fig. 2(b), where again the $y$ axis is compensated so that the plateau shows the range over which the scaling holds. Recognizing that this is a direct result of the quadratic dependence of cloud droplet removal rate on $r$, we can make the result more general by writing

$$m = \frac{\rho_l \xi s_0}{D'} \frac{\tau_{\rm res}}{\tau_t}. \tag{24}$$

Thus, in the polluted cloud, fast-microphysics limit, the observed liquid water content is essentially controlled by the ratio of the residence time of droplets to the flux replenishment time. Along with the Damkoehler number $\tau_t/\tau_c$, the dimensionless particle removal rate $\tau_t/\tau_{\rm res}$ can therefore be considered one of the key parameters governing the microphysical state of the system.

Unique expressions for the microphysical state of the system can be obtained by combining the above results from the mass balance with the number balance given by Eq. (14). Eliminating $n$ or $r$ from Eq. (22) results in

$$r = \left(\frac{3\xi s_0}{4\pi D'\dot{n}_{\rm in}\tau_t}\right)^{1/3} \tag{25}$$

and

$$n = \frac{9\mu H}{2\rho_l g}\left(\frac{4\pi D'\tau_t}{3\xi s_0}\right)^{2/3} \dot{n}_{\rm in}^{5/3}, \tag{26}$$

and from Eq. (23)

$$m = \frac{6\pi\mu H}{g}\left(\frac{3\xi s_0}{4\pi D'\tau_t}\right)^{1/3} \dot{n}_{\rm in}^{2/3}. \tag{27}$$

The power-law dependence on $\dot{n}_{\rm in}$ can be seen in the second and fourth panels of Fig. 1, where the number concentration curve has a slope of 5/3 and the liquid water content curve has a slope of 2/3 in log-log coordinates. Given that under a wide range of cloud conditions the fast-microphysics limit is valid, these remarkably simple expressions provide a convenient description of how the microphysical state of the system

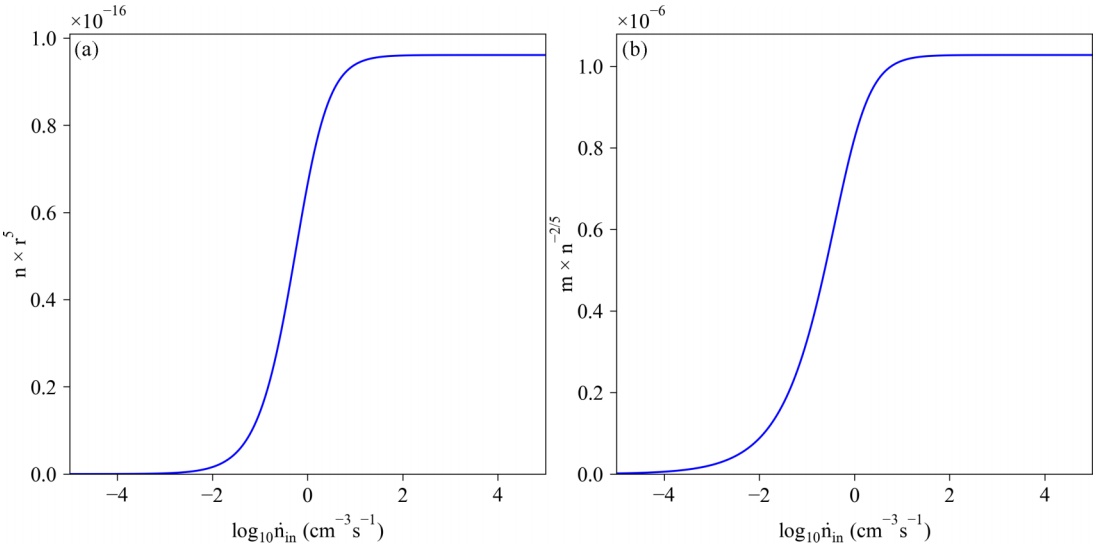


FIG. 2. Left panel illustrates $n \propto r^{-5}$ and right panel illustrates $m \propto n^{2/5}$ in the fast-microphysics limit ($\tau_t \gg \tau_c$). In this illustration, the fast microphysics regime is attained by increasing the injection rate of number of droplets. The parameters $\tau_t = 10$ s and $s_0 = 21.32\%$ are held constant.

depends on external parameters. This will be further explored in Sec. IV E.

### B. Slow-microphysics limit

We now consider the limit of slow microphysics (i.e., low CCN injection rate) compared to turbulent mixing, i.e., $\tau_t \ll \tau_c$. In that regime Eq. (10) can be expanded to first order so that $s \approx s_0(1 - \tau_t/\tau_c)$. Then the mass condensation rate is

$$\dot{m}_{\rm cond} = n\rho_l 4\pi r \xi s_0 (1 - \tau_t 4\pi D' n r), \tag{28}$$

and equating $\dot{m}_{\rm cond} = \dot{m}_{\rm sed}$ results in

$$n\rho_l 4\pi r \xi s_0 (1 - \tau_t 4\pi D' n r) = \frac{m}{\tau_{\rm res}}. \tag{29}$$

Using $\tau_{\rm res} = H/v_T$ and the Stokes drag law, this can be solved for cloud droplet number concentration

$$n = \frac{1}{4\pi D' r \tau_t}\left(1 - \frac{2\rho_l g r^4}{27\mu H \xi s_0}\right). \tag{30}$$

Solving instead for cloud liquid water content, the result is

$$m = \frac{\rho_l r^2}{3D'\tau_t}\left(1 - \frac{2\rho_l g r^4}{27\mu H \xi s_0}\right). \tag{31}$$

The clean cloud, slow-microphysics limit, when taken to the extreme of $\tau_t/\tau_c \to 0$ leads to an expression for droplet radius that is independent of number concentration,

$$r = \left(\frac{27\mu H \xi s_0}{2\rho_l g}\right)^{1/4}. \tag{32}$$

Effectively, this is the mean radius of isolated droplets growing in an environment with supersaturation $s_0$ during lifetime $\tau_{\rm res}$. The third panel of Fig. 1 shows a plateau at small $\dot{n}_{\rm in}$, confirming that this indeed is an upper limit to the droplet size achievable in a convection-cloud chamber. This leads to the interesting possibility that a measurement of mean droplet diameter in a convection-cloud chamber, operating with extremely low CCN injection rates, could provide an indirect measure of the maximum supersaturation $s_0$. Or, alternately, if the thermodynamic state is known, it could be used to explore the physics of droplet removal, i.e., to what extent the simple Stokes settling through the full chamber height $H$ quantitatively describes the particle lifetime.

Finally, bringing in the number budget Eq. (14) and using the maximum radius given by Eq. (32), it follows that in the extreme slow-microphysics limit both the cloud droplet number concentration and the liquid water content are directly proportional to the CCN injection rate, $n \propto \dot{n}_{\rm in}$ and $m \propto \dot{n}_{\rm in}$. These power-law relations (slope of 1) are observed in the low-$\dot{n}_{\rm in}$ ranges of the second and fourth panels of Fig. 1.

Figure 3 provides an alternate perspective on fast- and slow-microphysical regimes. Here, the microphysical state of the system is altered by varying the turbulent flux time scale $\tau_t$. The CCN injection rate is fixed, so the system changes from the slow microphysics $\tau_t \ll \tau_c$ to the fast microphysics $\tau_t \gg \tau_c$ regimes. The fourth panel shows $\tau_c$, and confirms that the transition from one regime to the other occurs near $\tau_t \approx \tau_c$. The droplet radius is observed to reach a maximum value as anticipated by Eq. (32).

### C. Energetic aspects of condensation

Here we consider the heating of the air in the cloud chamber as a result of cloud formation and associated latent heating. The temperature evolution equation is

$$\frac{dT}{dt} = -\frac{T - T_0}{\tau_t} + \frac{L}{c_p}\dot{q}_{l,cond}, \tag{33}$$

where $q_l = m/\rho_a$ is the liquid water mixing ratio. The additional subscript makes clear that only changes in liquid water mixing ratio resulting from condensation or evaporation are included. In steady state the time derivative is zero, so we can

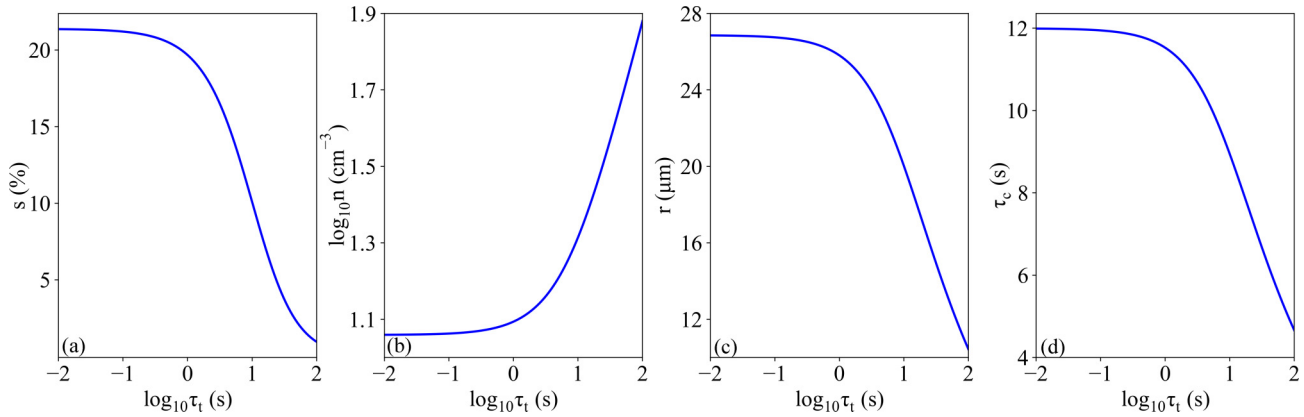


FIG. 3. The turbulence time scale $\tau_t$ is varied, with $\dot{n}_{\rm in} = 1\,{\rm cm}^{-3}\,{\rm s}^{-1}$ and $H = 1$ m held constant. Increase in $\tau_t$ results in a decrease in the rate of replenishment of the temperature and water vapor scalar fields. For the same droplet injection rate and $H$, the supersaturation decreases as $\tau_t$ increases.

solve for $\delta T = T - T_0$ as

$$\delta T = \frac{L}{\rho_a c_p}\dot{m}_{\rm cond}\tau_t. \tag{34}$$

The dependence of $\delta T$ on CCN injection rate $\dot{n}_{\rm in}$ is shown in Fig. 4, where it is clearly seen that a transition occurs between very clean versus polluted conditions. Using the fast-microphysics limit given by Eq. (21) we obtain

$$\delta T = \frac{L}{\rho_a c_p}\frac{\rho_l \xi s_0}{D'}. \tag{35}$$

It is interesting to note here that the temperature offset in this limit is independent of $\tau_t$; in other words, it is independent of the boundary fluxes. In contrast, in the slow-microphysics limit given by Eq. (28) we obtain

$$\delta T = \frac{L}{\rho_a c_p}\tau_t n\rho_l 4\pi r\xi s_0(1 - \tau_t 4\pi D' nr). \tag{36}$$

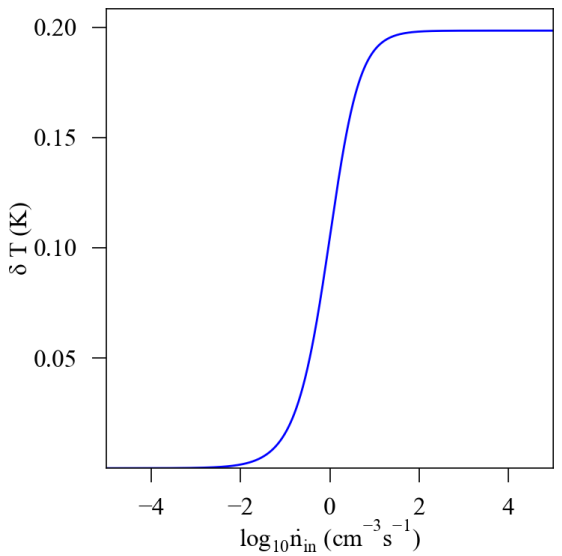


FIG. 4. Steady-state $\delta T$ vs droplet injection rate. The parameters are the same as in Fig. 1.

In the extreme limit of $\tau_c \to \infty$ this simplifies to

$$\delta T = \frac{L}{\rho_a c_p}\tau_t n\rho_l 4\pi r\xi s_0, \tag{37}$$

with the result that $\delta T \propto \tau_t$. It follows, because this result holds for small $\tau_t$, that $\delta T$ becomes vanishingly small as the microphysics becomes slower. In essence, the microphysics are sufficiently sluggish that the boundary fluxes are able to maintain the temperature near $T_0$ in spite of the latent heat release associated with cloud formation.

### D. Optical properties and the Twomey effect

The optical properties of a cloud scale with the optical depth $\tau \approx 2\pi nr^2$. The susceptibility is defined as $d\ln\tau/d\ln n$, and can be compared to the value of $1/3$ for the Twomey effect [27]. In the fast-microphysics limit we can rearrange Eq. (22) to obtain an expression with $r \sim n^{-1/5}$. The resulting susceptibility is

$$\frac{d\ln\tau}{d\ln n} = \frac{3}{5}, \tag{38}$$

which is significantly stronger than the classic Twomey value. In the slow-microphysics limit the radius is independent of $n$, as shown by Eq. (32). Therefore, the susceptibility is simply

$$\frac{d\ln\tau}{d\ln n} = 1. \tag{39}$$

It must be kept in mind that the susceptibility only takes on these values within the range of variation of $n$ safely within the assumed limits. In either case, however, we see that for this analytical model, the aerosol-indirect effect is quite strong. The enhancement above the Twomey value of $1/3$ can be understood as resulting from the change in liquid water content. Specifically, the optical depth can be written as $\tau \propto m^{2/3}n^{1/3}k^{1/3}h$, where $k$ is a dispersion coefficient and $h$ is the cloud thickness. In this case, the size distribution is simplified as monodisperse, so there is no effect of $k$, and the cloud thickness is fixed. The susceptibility then takes the form [28]

$$\frac{d\ln\tau}{d\ln n} = \frac{1}{3} + \frac{2d\ln m}{3d\ln n}. \tag{40}$$

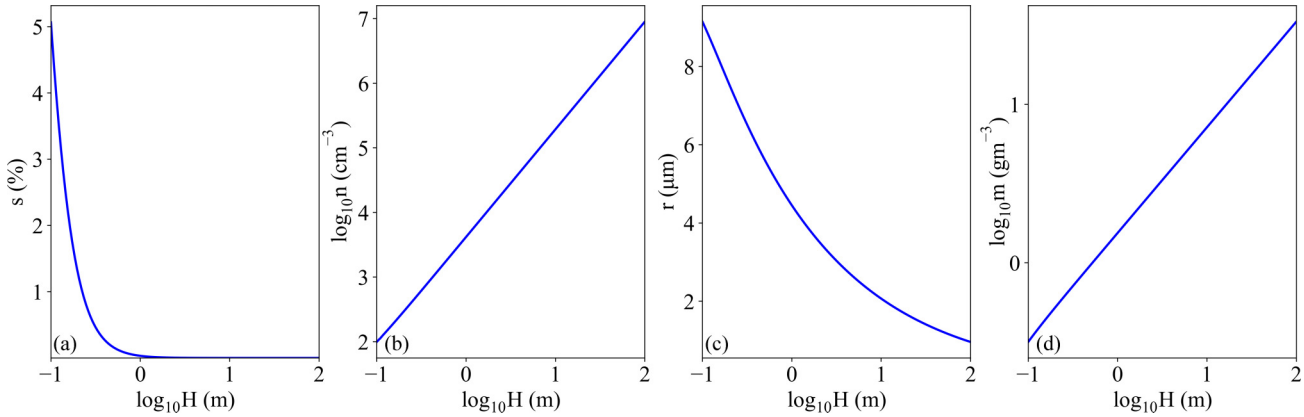


FIG. 5. The free parameter $H$ is changed with $\dot{n}_{\rm in} = 10\,{\rm cm}^{-3}\ {\rm s}^{-1}$, $\lambda = 5 \times\ 10^{-3}$ m, and $\delta = H$ m are held constant. For a given scalar flux, increase in $H$ results in longer time for replenishment of scalar. Larger $H$ results in longer residence time of the droplets, therefore more droplets are sustained in the system resulting in smaller supersaturation and droplet radius.

In the convection-cloud system, therefore, we see that the change in liquid water content $m$ with droplet concentration $n$ makes a significant contribution to the optical properties.

### E. Scaling with convective-layer height

In the context of Rayleigh-Bénard convection or a convection-cloud chamber, it is of interest to consider how cloud microphysical properties scale with system parameters. Externally controlled parameters are the imposed temperature difference $\Delta T$, which determines $s_0$, the aerosol injection rate $\dot{n}_{\rm in}$, and the system height $H$. We are interested in how the droplet radius $r$, droplet concentration $n$, and liquid water content $m$ vary. In this section we explore the dependence on convective-layer depth $H$.

Recall that the coefficients of the quartic equation given by Eq. (15) depend on $H$, which enters through the droplet residence time $\tau_{\rm res} = v_T/H$. It should also be noted that there is a further $H$ dependence in $\tau_t$. This turbulent transport time entered through the supersaturation equation (10), which can be written to show the dependence on $H$,

$$s = s_0\left(1 + \frac{2\pi H\lambda D' nr}{\alpha}\right)^{-1}. \tag{41}$$

Solutions for the microphysical state of the system as a function of $H$ are illustrated in Fig. 5, showing $s$, $n$, $r$, and $m$. Three decades of variation in $H$ is depicted in order to demonstrate the behavior of the system. The trends are consistent with those observed in more detailed large eddy simulation of convection-cloud chambers with varying height [29].

More insight into the behavior of the system can be gained by noting the distinct power laws observed in Fig. 5. Because $\tau_t$ scales linearly as $H$, most of the range shown satisfies the condition $\tau_c \ll \tau_t$. In this fast-microphysics limit we can obtain scaling relations from Eqs. (25)–(27). We simplify the expressions so that they only depend on parameters that can be externally controlled, including the height of a chamber $H$, the maximum supersaturation $s_0$, which is determined by the imposed temperature difference $\Delta T$, and the aerosol injection rate $\dot{n}_{\rm in}$. We replace $\tau_t$ here with $H$, and where particle removal rate enters, we write the linear scaling with $H$. The resulting scaling relations are

$$r \sim \left(\frac{s_0}{\dot{n}_{\rm in} H}\right)^{1/3}, \tag{42}$$

$$n \sim \frac{(H\dot{n}_{\rm in})^{5/3}}{s_0^{2/3}}, \tag{43}$$

and

$$m \sim (H\dot{n}_{\rm in})^{2/3} s_0^{1/3}. \tag{44}$$

These power-law relations on $H$ are observed in the right three panels of Fig. 5. The droplet concentration $n$ and liquid water content $m$ are observed to increase monotonically with power-law exponents of $5/3$ and $2/3$ as predicted for the limit of fast microphysics. Of course these scaling relations assume fixed boundary forcing $\Delta T$ and intensive aerosol injection rate $\dot{n}_{\rm in}$.

## V. VALIDATION WITH SIMULATION AND MEASUREMENTS

In this section we make two assessments of the theory and scaling laws developed thus far. First, we compare the theory to a computational solution to the governing equations. Second, we compare one of the key scaling laws with the measurements from the Pi chamber.

### A. Comparison with full ODE solutions

The simple model can be expressed as a set of coupled ordinary differential equations, without using the first-order approximation for supersaturation fluctuations used in Eqs. (B2) and (B3). In addition, numerical solution of the coupled set allows transient behavior to be investigated, and provides an opportunity to check consistency with the steady-state solutions obtained thus far. For cloudy Rayleigh-Bénard convection the time evolution equations for temperature, water vapor, liquid water content, and number concentration are given by

$$\frac{\partial T}{\partial t} = \frac{T_0 - T}{\tau_t} + \frac{L}{c_p} q\dot{l}_c, \tag{45}$$

$$\frac{\partial q_v}{\partial t} = \frac{q_{v0} - q_v}{\tau_t} - \dot{q_{l}}_c, \tag{46}$$

$$\frac{\partial q_l}{\partial t} = \dot{q_{l}}_t - \frac{q_l}{\tau_{\rm res}}, \tag{47}$$

$$\frac{\partial n}{\partial t} = \dot{n}_{\rm in}\mathcal{H}(s(t) - s_c) - \frac{n}{\tau_{\rm res}}, \tag{48}$$

with

$$\dot{q_{l}}_c = 4\pi n(t)\bar{r}(t)\xi s(t), \tag{49}$$

$$\dot{q_{l}}_t = 4\pi n(t)\bar{r}(t)\xi s(t) + \tfrac{4}{3}\pi\bar{r}(t)^3\rho_l\dot{n}_{\rm in}, \tag{50}$$

and

$$s(t) = \frac{q_v(t)}{q_{\rm sat}(t, T)}, \tag{51}$$

$$\bar{r}(t) = \left(\frac{3q_l(t)}{4\pi\rho_l n(t)}\right)^{1/3}, \tag{52}$$

where $s(t)$ is the time-dependent supersaturation, $\bar{r}(t)$ is the mean cloud droplet radius at time $t$, and $\mathcal{H}$ is the Heaviside step function. The first term in Eqs. (45) and (46) is the source term due to the turbulent flux transfer from the boundaries and subsequent mixing. This term tends to reduce the quasi-steady temperature and increase the quasi-steady water vapor in the bulk. The increase in bulk temperature due to latent heat release and a consequent reduction in bulk water vapor due to condensation is captured in the second term of Eqs. (45) and (46).

The $\dot{n}_{\rm in}$ in Eq. (48) represents the injection of cloud droplets when instantaneous supersaturation exceeds critical supersaturation ($s_c$). In a physical system, there is a finite time between the activation of droplets and growth to size $\bar{r}(t)$, but here the cloud droplet population is represented only by the mean size in order to stay close to the idealized model derived previously. Because liquid water mixing ratio is $q_l \propto nr^3$, its rate of change has two contributions, $\dot{q}_l \propto \dot{n}r^3 + 3nr^2\dot{r}$. Thus, in the set of ODEs, changes in liquid water content can arise from condensation/evaporation of existing droplets $\dot{q_{l}}_c$ and from injection $\dot{n}_{\rm in}$ of droplets of size $\bar{r}(t)$. These combined effects are represented by the first term $\dot{q_{l}}_t$ in Eq. (47), which is defined in Eq. (50). Only the condensation component $\dot{q_{l}}_c$ contributes to the temperature and water vapor fields described by Eqs. (45) and (46). This condensation term accounts for integrated growth over the full size distribution, which is represented just by the mean size. The sink term for both number and liquid water content is due to the droplet removal, with a characteristic time scale of $\tau_{\rm res}$. This exponential removal is captured by the second term in Eqs. (47) and (48).

In the system of ODEs, the direct coupling between the scalar fields $T$ and $q_v$ [Eqs. (45) and (46)], and microphysics [Eqs. (47) and (48)] is through the changes in temperature via latent heat release and in water vapor via condensation growth. A feedback to microphysics is established via changes in supersaturation and radius. The system of ODEs is solved with temperature and water vapor initialized with the no-cloud conditions $q_{v0}$ and $T_0$ for the convective system with $\Delta T$, and with liquid water content and number concentration both having initial conditions set to near zero ($10^{-18}$). The model parameters are $\dot{n}_{\rm in}$, $\tau_t$, and $H$ (which determines $\tau_{\rm res}$). An example of the transient response of the coupled system is given in Fig. 6, which shows the time evolution of supersaturation, liquid water content, droplet number concentration, and droplet mean radius. The system is initialized at the steady conditions that exist in the chamber when no aerosol particles are present, i.e., supersaturation of approximately 20%, corresponding to a mean temperature of 283.77 K and $\Delta T = 20$ K. The results displayed are for $\dot{n}_{\rm in} = 100$ cm$^{-3}$ s$^{-1}$, $\tau_t = 10$ s, and $H = 1$ m. Aerosol injection starts at $t = 0$ and the system is observed to reach steady state within approximately 10 s, and the observed values of $s$, $q_l$, $n$, and $r$ match the values given by the analytical, steady-state model [shown as red dashed lines, obtained using Eqs. (10), (14), and (15)]. When the system is in steady state, between approximately 20 and 60 s, the radius of 5.7 μm corresponds to a terminal speed of 3.6 mm s$^{-1}$, and therefore a residence time of approximately 276 s. At $t = 60$ s the aerosol injection is switched off and the liquid water content and droplet number concentration drop off, the supersaturation relaxes back to the no-cloud steady state, and the radius of remaining cloud droplets grows to to the maximum size predicted by the analytical theory [see Eq. (32), shown as the green dotted line].

### B. Comparison to measurements

Although the emphasis of this paper is on the theoretical development, we make an initial comparison of the theory to measurements performed in a convection-cloud chamber. The fast-microphysics regime is most readily achieved in the experiments, so we compare to the liquid-water scaling derived in Sec. IV A, specifically the dependence on aerosol injection rate given by Eqs. (27) and (44). We were able to vary the aerosol injection rate over a factor of approximately 100 in order to obtain a rigorous assessment of the power-law prediction. The slow-microphysics regime is challenging to access because of limitations in the ability to measure the droplet size distribution (i.e., due to the upper size limit imposed by the sampling tube of the droplet sizing instrument, the Welas 2000 by Palas GmbH).

Experiments were carried out in the Pi convection-cloud chamber [23]. A turbulent, supersaturated environment was created by setting up an unstable temperature difference across the top and bottom plates. The bottom plate was set to 30 °C and the top plate was set to 11 °C. The sidewall temperature was set to 20 °C, close to the average value of the top and bottom plates. Additionally, 20 °C, a value close to the room temperature was chosen as the sidewall temperature to minimize the heat leakage from the room to the sidewall cylinder. All boundaries were maintained at near saturated conditions. The chamber was seeded with sodium chloride aerosols, injected at a controlled rate to create the turbulent cloud environment. The cloud system reaches steady state when the injection rate of aerosols is balanced by the removal of cloud droplets by sedimentation. In order to achieve a broad range of injection rates, monodisperse, size-selected aerosols were used in the low range and polydisperse aerosols were used in the high range. The system reaches steady state in less than 30 minutes for all injection rates. The droplet size distribution was measured at intervals of 10 minutes starting from 30 minutes after injection. A total of seven samples were

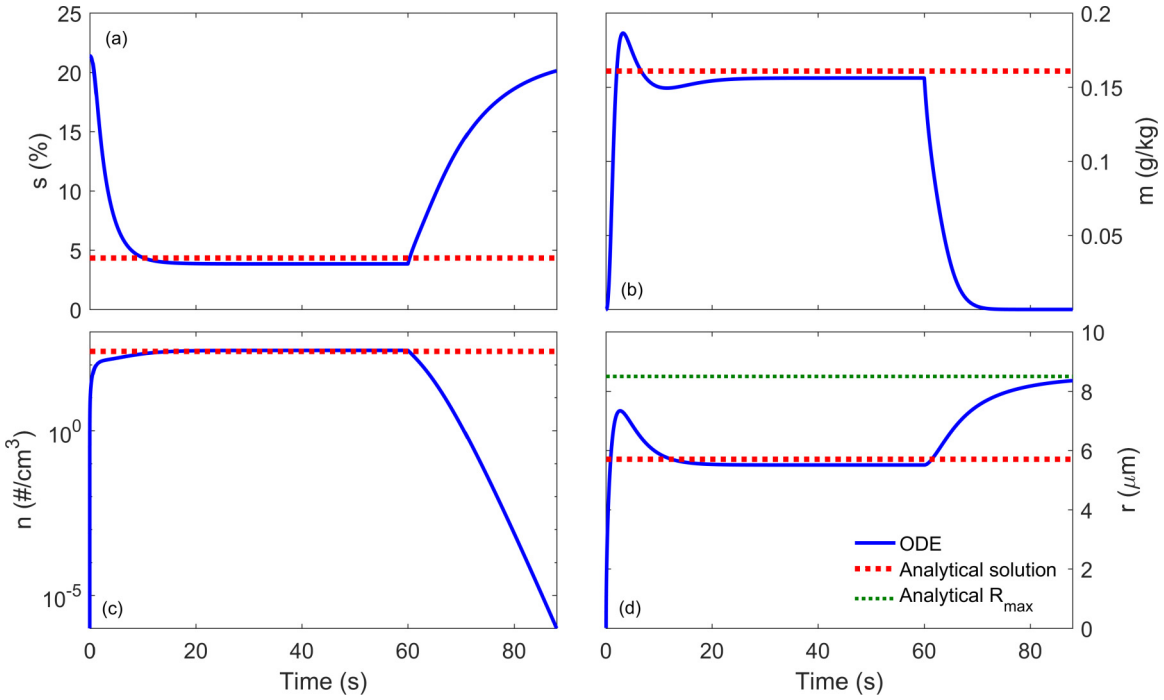


FIG. 6. Comparison of the ODE solutions (blue) with analytical solution (red dashed line). (a) Supersaturation, (b) liquid water content, (c) number concentration, and (d) radius are compared. The system is initialized at the steady-state conditions that exist in the chamber with no cloud droplets present and with aerosol injection starting at $t = 0$ s. At $t = 60$ s the injection is turned off and the cloud collapses. During the cloud collapse, the mean supersaturation increases and the droplet diameter increases, and consequently the droplet removal flux increases. The maximum droplet size obtained analytically (green dotted line) is reached as the droplet concentration becomes very small.

measured for all but three cases. The measurement was carried out using a WELAS 2000 digital optical particle counter in the size range of 0.6 to 40 μm. Each measurement was averaged over 100 seconds at a sampling rate of 5 liters per minute.

Figure 7 shows the liquid water content measured in the Pi chamber as a function of the activation rate. The activation rate was obtained from the interstitial/droplet concentration ($n_a/n_d$) budget. The interstitial concentration budget is written as

$$\frac{dn_a}{dt} = I - A - D, \tag{53}$$

where $I$ is the injection rate of aerosols, $A$ is the activation rate of the aerosols, and $D$ is the diffusive/sedimentation losses of the interstitials to the walls. The wall losses are represented as $n_a/\tau_a$. Solving Eq. (53) gives a solution $n_a(t) = \tau_a(I - A)(1 - \exp(-t/\tau_a))$. The time series of the interstitial number concentration evolution is obtained using a TSI scanning mobility particle sizer (SMPS). This data is used for obtaining the interstitial decay time constant $\tau_a$. Once $\tau_a$ is known we use Eq. (53) under steady-state conditions to obtain the activation rate $A = I - n_a/\tau_a$.

To evaluate the liquid water scaling in the fast-microphysics limit, as given by Eq. (44), we fit the data to a power law with exponent 2/3. The result is shown by the dotted line in Fig. 7. We use nonlinear least-square fitting with data points weighted by the measured uncertainties. The fit results in an acceptable $R^2$ value of 0.94. We note that a linear-least-square fit performed on the logarithm of the data points yields similarly encouraging results. We intend to conduct further evaluation of the theory against measurements in future work.

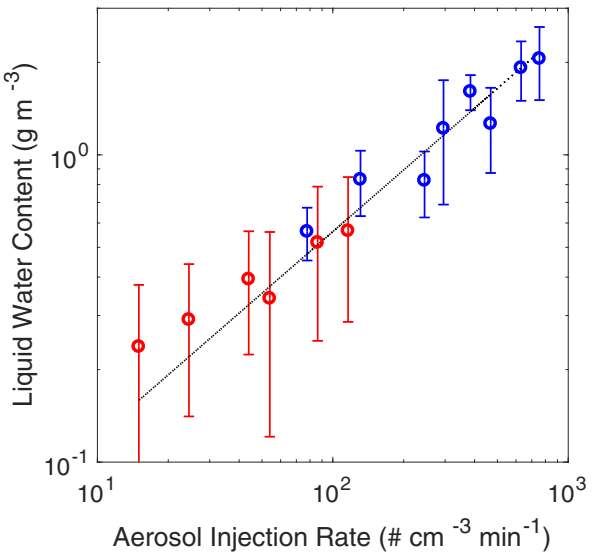


FIG. 7. Liquid water content versus CCN activation rate, measured in the Pi convection-cloud chamber. Low injection rates use size-selected CCN (red circles) and high injection rates are based on polydisperse CCN (blue circles). The uncertainty was determined by choosing the minimum and maximum value from all the samples for each case. The dotted line is a best-fit power law with exponent of 2/3, corresponding to Eq. (44).

## VI. DISCUSSION AND CONCLUDING REMARKS

We have developed a mean-field model of cloud microphysical properties in a steady-state turbulent mixed layer. The specific context is moist Rayleigh-Bénard convection inspired by the Pi convection-cloud chamber. The equations account for the adjustment of supersaturation to the steady aerosol injection rate. By considering number and mass balances, a quartic equation is obtained for mean droplet radius. Analytical expressions for cloud droplet radius, number concentration, and liquid water content are obtained for two limits of fast and slow microphysics compared to the turbulence flux time scale. The fast microphysics expressions are shown to compare favorably to measurements of liquid water content versus aerosol injection rate in the Pi convection-cloud chamber.

One insight to be taken from this paper is the value of developing idealized microphysical models that explicitly allow for finite supersaturation. This is in the spirit of the study by Porz *et al.* [30] in developing a sub-grid-scale model for cloud microphysical properties without saturation adjustment. Our mean-field approach was motivated by the findings of Krueger [20], who obtained closed-form expressions for the droplet size distribution shape by considering a balance between condensation growth and sedimentation. That model requires supersaturation to be specified; we expect that the approach taken here, using first and third moments, would allow the Krueger model to be closed, thereby enabling the supersaturation to be determined for a given aerosol injection rate.

Prior work has pointed toward the existence of fast- versus slow-microphysics regimes, based on the magnitudes of phase relaxation and turbulence time scales [18,31]. Naturally occurring clouds seem to reside primarily in the fast-microphysics regime, but *in situ* measurements with the holographic detector for clouds (HOLODEC) have shown that in the transition to open cellular convection characteristic of very clean, drizzling stratocumulus, the slow-microphysics regime can be approached [32]. Observations of liquid clouds in the pristine Arctic boundary layer by Mauritsen *et al.* [33] also show that large droplets can be produced without growth by collision–coalescence, which we consider as indicative of the slow-microphysics regime. We speculate that this growth limit is important to consider in clean regions, and may be lacking in current cloud parametrizations because in the slow regime the saturation adjustment assumption breaks down.

In the remainder of this section we first consider the relevant dimensionless quantities that appear in the quartic equation derived for droplet radius. We then make additional comments on connections to a bulk microphysics perspective, and on the central role played by the droplet removal rate. Finally, we conclude with a brief discussion of possibilities for extending this study.

### A. Generalization through dimensionless variables

To extend these results to different contexts we consider the dimensionless variables that contribute to the two limiting microphysical regimes. The natural radius for nondimensionalizing the problem is the size of an isolated droplet growing at maximum supersaturation $s_0$, given by Eq. (32). We will refer to this as $r_0$, and the dimensionless radius is denoted $\tilde{r} \equiv r/r_0$. We see that the last (constant) term in the governing quartic equation [Eq. (15)] is simply $-r_0^4$. Upon nondimensionalization, the coefficient of the $r^3$ term can be interpreted by recognizing the residence time of a droplet of radius $r_0$, namely $\tau_{res,0} = H/v_T(r_0) = 9\mu H/(2\rho_l g r_0^2)$. This leads naturally to an estimate of a reference droplet concentration via $n_0 = \dot{n}_{\rm in}\tau_{res,0}$. The $r^3$ coefficient then appears as a ratio of the turbulent mixing time scale $\tau_t$ and a phase relaxation time [cf. Eq. (9)] $\tau_{c,0} = (4\pi D' n_0 r_0)^{-1}$. It follows that the dimensionless form of Eq. (15), the governing quartic, is

$$\tilde{r}^4 + \frac{\tau_t}{\tau_{c,0}}\tilde{r}^3 - 1 = 0. \tag{54}$$

Alternatively, defining a Damkoehler number based on the phase relaxation time for the slow-microphysics limit $Da_0 = \tau_t/\tau_{c,0}$, the equation becomes

$$\tilde{r}^4 + Da_0\tilde{r}^3 - 1 = 0. \tag{55}$$

This is refreshingly simple and emphasizes the role of the Damkoehler number in the microphysical state of a cloudy mixed layer. It needs to be recognized, however, that this form of the equation masks the fundamental role of the droplet residence time, which in this case is embedded in $Da_0$ through the reference number concentration $n_0$. It also is crucial to note that the reference radius $r_0$ depends on the maximum supersaturation $s_0$, which in turn depends on $\Delta T$ or, more generally, the convective-layer forcing. Thus, the primary dimensionless variables governing the microphysical properties in this convective-layer model are the maximum supersaturation $s_0$ representing the "forcing" for droplet growth, the sedimentation parameter depending on the droplet residence time (sometimes referred to as Rouse number), and the Damkoehler number depending on the cloud phase relaxation time. This set is similar to that outlined by Thomas *et al.* [17]. Finally, it is intriguing to note that the reference radius $r_0$ is proportional to the fourth-root of the product $H\xi s_0$, which is similar to the dependence of the radius parameter for the gamma distribution derived by Krueger [20].

### B. Bulk microphysics perspective

The fast-microphysics limit of the mean-field model, e.g., Sec. IV, has a connection to the concept of saturation adjustment. In the analytical model, supersaturation is given by Eq. (10). In bulk microphysics models, however, saturation adjustment ensures that any supersaturation present is fully consumed by droplets present in a grid box [34]. This connection is outlined here, and will be further explored in future work.

The in-cloud steady-state temperature and water vapor mixing ratio are given by

$$T_s = T_0 + \tau_t \frac{L}{c_p}\dot{q}_l \tag{56}$$

and

$$q_{vs} = q_{v0} - \tau_t \dot{q}_l. \tag{57}$$

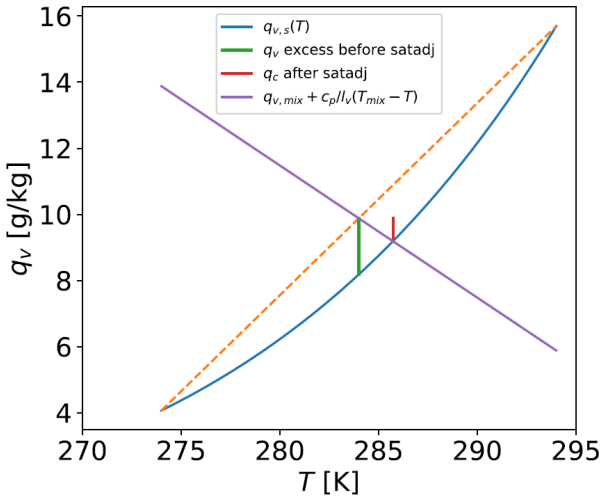


FIG. 8. The boundary conditions of the top and bottom plates lie on the Clausius-Clapeyron line (blue) and are connected by the mixing line (dashed orange). The initial excess water vapor (green) undergoes condensation (purple) until supersaturation goes to zero. The total mass of liquid water thus formed is equal to the mass water vapor removed (red).

With saturation adjustment, Eq. (57) reduces to

$$q_{v\,\mathrm{sat}}(T_s) = q_{v0} - \tau_t \dot{q}_l. \tag{58}$$

Adding Eq. (56) and $L/c_p \times$ Eq. (58) we have

$$T_s + \frac{L}{c_p} q_{v\,\mathrm{sat}}(T_s) = T_0 + \frac{L}{c_p} q_{v0}. \tag{59}$$

This equation can be solved for $T_s$ graphically as shown in Fig. 8, or numerically. For a saturation-adjusted system in steady state, the total condensed water and consequently the precipitated liquid water is given by the quantity $\tau_t \dot{q}_{l\,c}$. Thus by specifying the final steady-state equilibrium condition for the dynamical system to be saturated irrespective of the number of droplets, obviates the need of an equation for the number droplets.

The total liquid water content depends on both production via condensation and removal via settling. Assuming droplets are removed with a velocity of $v_T$,

$$q_l = \dot{q}_l \frac{H}{v_T}. \tag{60}$$

For droplets with low Reynolds number in the absence of turbulence coupling, the Stokes removal approximation for liquid water content is reasonable. We then obtain $q_l \sim n^{2/5}$, which is the same scaling as we obtained for the fast-microphysics regime discussed in Sec. IV. Fast microphysics implies that the droplets consume any supersaturation faster than the supersaturation generation process, which is consistent with the concept of saturation adjustment.

### C. Consideration of droplet removal rate

Removal of droplets through sedimentation at the Stokes terminal speed, while turbulence thoroughly mixes the bulk volume, leads to the stirred settling approximation with $\tau_{\mathrm{res}} = H/v_t$ [35]. This removal time scale has been used throughout this paper, and is fundamental in determining the steady-state microphysical conditions. Especially for large particles, where inertial effects are significant, this model may need to be refined [36]. Furthermore, when large droplets are present, the droplet fall speeds may approach or even exceed root-mean-square turbulence velocities. For example, in the Pi chamber, typical turbulence velocities are of order 1–10 cm/s, so droplets with radii exceeding ≈10 μm may not be well mixed within the turbulent layer.

To illustrate the critical role of this assumption, we consider a plausible alternate model: Assume that large droplets are only transported efficiently by turbulence over depth $\delta$ within the chamber, and from which they are removed by Stokes settling. For example, very large droplets that have a settling speed large compared to the characteristic turbulent velocity (i.e., large Rouse number) may reside primarily in the bottom part of the mixed layer. In this case, if we speculate that the residence time can be written as $\tau_{\mathrm{res}} = \delta/v_T$, it follows that Eq. (15) becomes

$$r^4 + \left(\frac{18\pi\mu\delta D' \tau_t \dot{n}_{\mathrm{in}}}{\rho_l g}\right) r^3 - \frac{27\xi\mu\delta s_0}{2\rho_l g} = 0. \tag{61}$$

This, in turn, would lead to modification of the subsequent equations, and in particular the $H$ dependencies explored in Sec. IV E would need to be modified. For this $\delta$ model in which there is no dependence on $H$ for the droplet removal time scale, the fast-microphysics scaling laws change to the following very different forms:

$$r \sim \left(\frac{s_0}{\dot{n}_{\mathrm{in}} \tau_t}\right)^{1/3}, \tag{62}$$

$$n \sim \delta \left(\frac{H}{s_0}\right)^{2/3} \dot{n}_{\mathrm{in}}^{5/3}, \tag{63}$$

and

$$m \sim \delta \left(\frac{s_0}{H}\right)^{1/3} \dot{n}_{\mathrm{in}}^{2/3}. \tag{64}$$

This simple model is speculative for very large radius, and is discussed here simply to underscore the importance of properly representing droplet-removal physics in order to obtain a proper representation of microphysical properties in a turbulent mixed layer.

### D. Future efforts

This paper opens the way to several interesting lines of continued investigation. Logical ways to expand on the results are to account for the full droplet size distribution, either through a more sophisticated treatment of moments, or by linking to the treatment of Krueger [20]. Another line of investigation is to make a more rigorous link to sub-grid-scale representations of supersaturation forcing, such as in eddy-diffusivity approaches [37,38]. Perhaps more challenging is to extend the model to include growth by collision and coalescence. The approach of Porz *et al.* [30] might be one possibility. It is likely, however, that inclusion of collision coalescence will make analytical solutions more challenging to obtain. These are some of the challenges that remain for adapting the minimalist model presented here to the atmospheric context. Nevertheless, as stated in Introduction, the

essential elements for a steady-state, mean-field model remain the same, regardless of context: supersaturation forcing term, steady source of aerosol, physics of droplet growth (by condensation, etc.), and physics of removal, e.g., by sedimentation. The size dependence of droplet growth and removal will alter details of the scaling laws obtained here, but slow- and fast-microphysics regimes will still exist.

We conclude by briefly discussing implications of this paper for research using convection-cloud chambers. One possible topic of interest for future experiments is to achieve droplet growth by collision–coalescence in addition to condensation. It is widely understood that the collision–coalescence process is favored when liquid water content is large, and when droplet diameters are large [26]. Of course the theoretical results in the main part of the paper, and the measurements presented in Sec. V B all demonstrate that liquid water content increases with aerosol injection rate, at least until the critical supersaturation discussed in Sec. III D is reached. This increase in $m$ is accomplished at the expense of decreasing $r$, however. The scaling laws derived for the fast-microphysics regime suggest that, for a given aerosol injection rate, liquid water content can be increased by increasing $s_0$, e.g., by increasing $\Delta T$ in a convection-cloud chamber, as well as by increasing $H$. A quantitative evaluation of when collision–coalescence becomes significant, and how it depends on these three variables, will be an intriguing possibility for future research.

## ACKNOWLEDGMENTS

This work was supported by National Science Foundation Grants No. AGS-1754244 and No. AGS-2133229, and by the U.S. Department of Energy's Atmospheric System Research, an Office of Science Biological and Environmental Research program. F.Y. has been funded by the Department of Energy (DOE) as part of the Atmospheric System Research (ASR) program under Contract No. DE-SC0012704. Pacific Northwest National Laboratory is operated by Battelle for the U.S. Department of Energy under Contract No. DE-AC05-76RL01830.

## APPENDIX A: SUPERSATURATION IN A CONVECTION-CLOUD CHAMBER

Here we consider a volume of the cylindrical convection chamber with a volume of $V = AH$, where $A$ and $H$ are the cross-sectional area and height of the chamber, respectively. Assuming $T$ is the air temperature of air in the well-mixed chamber, $T_b$ and $T_t$ are bottom and top surface temperatures. Based on energy conservation,

$$\rho_a c_p V \frac{dT}{dt} = (\Phi_b + \Phi_t) A_\Pi, \tag{A1}$$

where $\rho_a$ is the mass density of air and $c_p$ is the specific heat of air at constant pressure. The energy fluxes are due to thermal conduction through the viscous boundary layer with thickness $\lambda$, $\Phi_b = k(T_b - T)/\lambda$ and $\Phi_t = k(T_t - T)/\lambda$, where $k$ is the thermal conductivity of air. In practice, the boundary layer thickness can be estimated from the Nusselt number, $\mathrm{Nu} = H/\lambda$. The temperature equation then simplifies to

$$\frac{dT}{dt} = \frac{2\alpha}{H\lambda}(T_0 - T), \tag{A2}$$

where $\alpha$ is the thermal diffusivity of air and $T_0 = (T_b + T_t)/2$.

Under cloud-free conditions, the supersaturation in a convection chamber is denoted $s_0$ and this can be calculated directly from the imposed $\Delta T$. It is assumed that both boundaries are saturated, such that the vapor pressure at the top boundary is $e_t = e_s(T_t)$ and at the bottom boundary is $e_b = e_s(T_b)$. The mean vapor pressure is $\overline{e} = (e_t + e_b)/2$, and it follows that the supersaturation of the bulk fluid, which is at $\overline{T}$ and $\overline{e}$, is

$$s_0 = \frac{\overline{e}}{e_s(\overline{T})} - 1. \tag{A3}$$

Note that $\overline{T} = T_0$ from the main paper. Using the above definitions, we can write

$$s_0 = \frac{e_s(\overline{T} + \Delta T/2) + e_s(\overline{T} - \Delta T/2)}{2e_s(\overline{T})} - 1. \tag{A4}$$

We desire an approximate, analytical expression of $s_0(\Delta T)$, so we integrate the Clausius-Clapeyron equation, assuming the latent heat $L$ is a constant, resulting in $e_s(T) = A_e \exp(-L/R_v T)$, where $A_e$ is a constant. Assuming $\Delta T \ll \overline{T}$, we can write

$$e_s\left(\overline{T} \pm \frac{\Delta T}{2}\right) = A_e \exp\left(-\frac{L}{R_v \overline{T}}\right) \exp\left(\pm \frac{L\Delta T}{2R_v \overline{T}^2}\right). \tag{A5}$$

The supersaturation given by Eq. (A4) then becomes

$$s_0 = \frac{1}{2}\left[\exp\left(\frac{L\Delta T}{2R_v \overline{T}^2}\right) + \exp\left(-\frac{L\Delta T}{2R_v \overline{T}^2}\right)\right] - 1. \tag{A6}$$

The exponentials can be expanded to second order to preserve the curvature of the vapor-pressure function, which is necessary to represent supersaturation formation through mixing. The approximate expression for the cloud-free supersaturation then becomes

$$s_0 = \frac{1}{2}\left(\frac{L\Delta T}{2R_v \overline{T}^2}\right)^2. \tag{A7}$$

Note that this expansion requires $\Delta T \ll 2R_v \overline{T}^2/L$. For $\overline{T} = 290$ K this requirement becomes approximately $\Delta T \ll 30$ K. For $\Delta T = 10$ K the expression given by Eq. (A7) is good to about 10%.

The fundamental point here is that $s_0$ is a function of the boundary conditions $T_b$ and $T_t$ through $\Delta T$ and $\overline{T}$. Thus, the boundary conditions control both the turbulent fluxes of water vapor and thermal energy, and the resulting cloud-free supersaturation $s_0$.

## APPENDIX B: EQUATION FOR *ds/dt*

Because $s = s(q_v, T)$, the time rate of change of supersaturation is

$$\frac{ds}{dt} = \frac{\partial s}{\partial q_v}\frac{dq_v}{dt} + \frac{\partial s}{\partial T}\frac{dT}{dt}. \tag{B1}$$

The time rates of change of $q_v$ and $T$ given by Eqs. (1) and (3) contain the same time scale $\tau_t$, and can be substituted into Eq. (B1) to give

$$\frac{ds}{dt} = \frac{1}{\tau_t}\left[\frac{\partial s}{\partial q_v}(q_{v0} - q_v) + \frac{\partial s}{\partial T}(T_0 - T)\right]. \quad \text{(B2)}$$

If we take the partial derivatives $\partial s/\partial q_v$ and $\partial s/\partial T$ as constants evaluated at $(q_{v0}, T_0)$, then the right-hand side has the form of a Taylor expansion around $s_0$,

$$s = s_0 + \frac{\partial s}{\partial q_v}\Big|_{q_{v0},T_0}(q_v - q_{v0}) + \frac{\partial s}{\partial T}\Big|_{q_{v0},T_0}(T - T_0). \quad \text{(B3)}$$

Since the term in square brackets in Eq. (B2) can be replaced with $s - s_0$ by using Eq. (B3), it then follows that $ds/dt = (s_0 - s)/\tau_t$, which is Eq. (4). At this level of approximation, therefore, we can treat supersaturation as a simple scalar field forced by the water vapor and thermal energy fluxes from the boundaries. It should be noted that only a first-order expansion is needed here, in contrast to the derivation leading to Eq. (A7), because the expansion is for small deviations from $s_0$ and the shape of the Clausius-Clapeyron function does not matter. The adequacy of this approximation is checked both computationally and experimentally in Sec. V.


[1] D. K. Lilly, Models of cloud-topped mixed layers under a strong inversion, Q. J. R. Meteorolog. Soc. **94**, 292 (1968).

[2] J. Deardorff, On the entrainment rate of a stratocumulus-topped mixed layer, Q. J. R. Meteorolog. Soc. **102**, 563 (1976).

[3] W. H. Schubert, Experiments with Lilly's cloud-topped mixed layer model, J. Atmos. Sci. **33**, 436 (1976).

[4] C. Chen and W. R. Cotton, A one-dimensional simulation of the stratocumulus-capped mixed layer, Boundary Layer Meteorol. **25**, 289 (1983).

[5] S. Nicholls, The dynamics of stratocumulus: Aircraft observations and comparisons with a mixed layer model, Q. J. R. Meteorolog. Soc. **110**, 783 (1984).

[6] S. T. Siems, D. H. Lenschow, and C. S. Bretherton, A numerical study of the interaction between stratocumulus and the air overlying it, J. Atmos. Sci. **50**, 3663 (1993).

[7] B. Stevens, Entrainment in stratocumulus-topped mixed layers, Q. J. R. Meteorolog. Soc. **128**, 2663 (2002).

[8] J. P. Mellado, The evaporatively driven cloud-top mixing layer, J. Fluid Mech. **660**, 5 (2010).

[9] S. R. De Roode, A. P. Siebesma, S. Dal Gesso, H. J. Jonker, J. Schalkwijk, and J. Sival, A mixed-layer model study of the stratocumulus response to changes in large-scale conditions, J. Adv. Model. Earth Syst. **6**, 1256 (2014).

[10] F. Hoffmann, F. Glassmeier, T. Yamaguchi, and G. Feingold, Liquid water path steady states in stratocumulus: Insights from process-level emulation and mixed-layer theory, J. Atmos. Sci. **77**, 2203 (2020).

[11] T. Schneider, J. Teixeira, C. S. Bretherton, F. Brient, K. G. Pressel, C. Schär, and A. P. Siebesma, Climate goals and computing the future of clouds, Nat. Clim. Change **7**, 3 (2017).

[12] I. Boutle and S. Abel, Microphysical controls on the stratocumulus topped boundary-layer structure during vocals-rex, Atmos. Chem. Phys. **12**, 2849 (2012).

[13] F. Hoffmann and G. Feingold, Entrainment and mixing in stratocumulus: Effects of a new explicit subgrid-scale scheme for large-eddy simulations with particle-based microphysics, J. Atmos. Sci. **76**, 1955 (2019).

[14] K. K. Chandrakar, H. Morrison, and M. Witte, Evolution of droplet size distributions during the transition of an ultraclean stratocumulus cloud system to open cell structure: An LES investigation using Lagrangian microphysics, Geophys. Res. Lett. **49**, e2022GL100511 (2022).

[15] G. Young, P. J. Connolly, H. M. Jones, and T. W. Choularton, Microphysical sensitivity of coupled springtime arctic stratocumulus to modelled primary ice over the ice pack, marginal ice, and ocean, Atmos. Chem. Phys. **17**, 4209 (2017).

[16] C. Wainwright and D. Richter, Investigating the sensitivity of marine fog to physical and microphysical processes using large-eddy simulation, Boundary Layer Meteorol. **181**, 473 (2021).

[17] S. Thomas, P. Prabhakaran, F. Yang, W. H. Cantrell, and R. A. Shaw, Dimensionless parameters for cloudy Rayleigh-Bénard convection: Supersaturation, Damköhler, and Nusselt numbers, Phys. Rev. Fluids **7**, 010503 (2022).

[18] K. K. Chandrakar, W. Cantrell, K. Chang, D. Ciochetto, D. Niedermeier, M. Ovchinnikov, R. A. Shaw, and F. Yang, Aerosol indirect effect from turbulence-induced broadening of cloud-droplet size distributions, Proc. Natl. Acad. Sci. USA **113**, 14243 (2016).

[19] P. Prabhakaran, A. S. M. Shawon, G. Kinney, S. Thomas, W. Cantrell, and R. A. Shaw, The role of turbulent fluctuations in aerosol activation and cloud formation, Proc. Natl. Acad. Sci. USA **117**, 16831 (2020).

[20] S. K. Krueger, Equilibrium droplet size distributions in a turbulent cloud chamber with uniform supersaturation, Atmos. Chem. Phys. **20**, 7895 (2020).

[21] S. Thomas, M. Ovchinnikov, F. Yang, D. van der Voort, W. Cantrell, S. K. Krueger, and R. A. Shaw, Scaling of an atmospheric model to simulate turbulence and cloud microphysics in the Pi chamber, J. Adv. Model. Earth Syst. **11**, 1981 (2019).

[22] P. Prabhakaran, S. Thomas, W. Cantrell, R. A. Shaw, and F. Yang, Sources of stochasticity in the growth of cloud droplets: Supersaturation fluctuations versus turbulent transport, J. Atmos. Sci. **79**, 3145 (2022).

[23] K. Chang, J. Bench, M. Brege, W. Cantrell, K. Chandrakar, D. Ciochetto, C. Mazzoleni, L. Mazzoleni, D. Niedermeier, and R. Shaw, A laboratory facility to study gas–aerosol–cloud interactions in a turbulent environment: The $\pi$ chamber, Bull. Am. Meteorol. Soc. **97**, 2343 (2016).

[24] D. Lamb and J. Verlinde, *Physics and Chemistry of Clouds* (Cambridge University Press, Cambridge, 2011).

[25] J. G. Crump and J. H. Seinfeld, Turbulent deposition and gravitational sedimentation of an aerosol in a vessel of arbitrary shape, J. Aerosol Sci. **12**, 405 (1981).

[26] R. Rogers and M. Yau, *A Short Course in Cloud Physics.* (Pergamon, New York, 1989).

[27] S. Platnick and S. Twomey, Determining the susceptibility of cloud albedo to changes in droplet concentration with the

advanced very high resolution radiometer, J. Appl. Meteorol. Climatol. **33**, 334 (1994).

[28] K. Chandrakar, W. Cantrell, A. Kostinski, and R. Shaw, Dispersion aerosol indirect effect in turbulent clouds: Laboratory measurements of effective radius, Geophys. Res. Lett. **45**, 10 (2018).

[29] S. Thomas, F. Yang, M. Ovchinnikov, W. Cantrell, and R. A. Shaw, Scaling of turbulence and microphysics in a convection–cloud chamber of varying height, J. Adv. Model. Earth Syst. **15**, e2022MS003304 (2023).

[30] N. Porz, M. Hanke, M. Baumgartner, and P. Spichtinger, A model for warm clouds with implicit droplet activation, avoiding saturation adjustment, Math. Clim. Weather Forecasting **4**, 50 (2018).

[31] C. Siewert, J. Bec, and G. Krstulovic, Statistical steady state in turbulent droplet condensation, J. Fluid Mech. **810**, 254 (2017).

[32] N. Desai, S. Glienke, J. Fugal, and R. Shaw, Search for microphysical signatures of stochastic condensation in marine boundary layer clouds using airborne digital holography, J. Geophys. Res.: Atmos. **124**, 2739 (2019).

[33] T. Mauritsen, J. Sedlar, M. Tjernström, C. Leck, M. Martin, M. Shupe, S. Sjogren, B. Sierau, P. Persson, I. Brooks *et al.*, An Arctic CCN-limited cloud-aerosol regime, Atmos. Chem. Phys. **11**, 165 (2011).

[34] A. Khain, K. Beheng, A. Heymsfield, A. Korolev, S. Krichak, Z. Levin, M. Pinsky, V. Phillips, T. Prabhakaran, A. Teller *et al.*, Representation of microphysical processes in cloud-resolving models: Spectral (bin) microphysics versus bulk parameterization, Rev. Geophys. **53**, 247 (2015).

[35] J. G. Crump, R. C. Flagan, and J. H. Seinfeld, Particle wall loss rates in vessels, Aerosol Sci. Technol. **2**, 303 (1982).

[36] D. Richter and M. Chamecki, Inertial effects on the vertical transport of suspended particles in a turbulent boundary layer, Boundary Layer Meteorol. **167**, 235 (2018).

[37] I. Lopez-Gomez, Y. Cohen, J. He, A. Jaruga, and T. Schneider, A generalized mixing length closure for eddy-diffusivity mass-flux schemes of turbulence and convection, J. Adv. Model. Earth Syst. **12**, e2020MS002161 (2020).

[38] K. Suselj, J. Teixeira, M. J. Kurowski, and A. Molod, Improving the representation of subtropical boundary layer clouds in the nasa geos model with the eddy-diffusivity/mass-flux parameterization, Mon. Weather Rev. **149**, 793 (2021).